LANGMUIR

pubs.acs.org/Langmuir Article

Versatile Surface Functionalization of Water-Dispersible Iron Oxide Nanoparticles with Precisely Controlled Sizes

Pohlee Cheah, Paul Brown, Jing Qu, Bin Tian, Derek L. Patton, and Yongfeng Zhao*

Cite This: https://dx.doi.org/10.1021/acs.langmuir.0c03314 Read Online

ACCESS | Metrics & More | Article Recommendations | Supporting Information

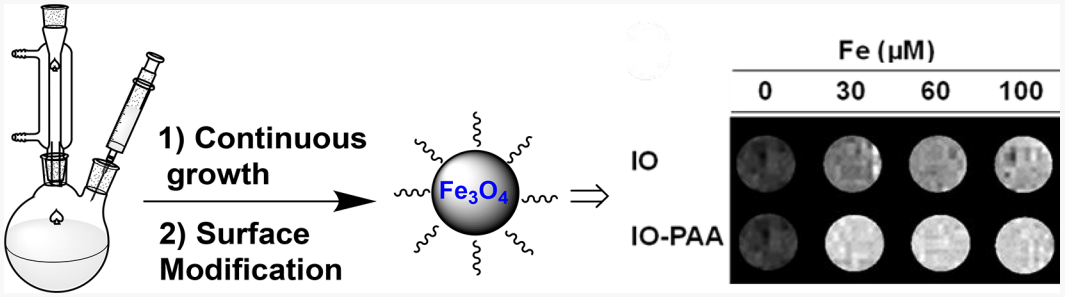

ABSTRACT: The synthesis of highly water-dispersible iron oxide nanoparticles with surface functional groups and precisely controlled sizes is essential for biomedical application. In this paper, we report a one-pot strategy for versatile surface functionalization. The iron oxide nanoparticles are first synthesized by thermal decomposition of iron(III) acetylacetonate ($Fe(acac)_3$) in diethylene glycol (DEG), and their surfaces are modified by adding the surface ligands at the end of the reaction. The size of iron oxide nanoparticles can be precisely controlled in nanometer scale by continuous growth. This facile synthesis method enables the surface modification with different coating materials such as dopamine (DOPA), polyethylene glycol with thiol end group (thiol-PEG), and poly(acrylic acid) (PAA) onto the iron oxide nanoparticles, introducing new surface functionalities for future biomedical application. From transmission electron microscopy (TEM) and X-ray diffraction (XRD), the morphology and crystal structure are not changed during surface functionalization. The attachment of surface ligands is studied by Fourier transform infrared spectroscopy (FTIR) and Thermogravimetric Analysis (TGA). The surface functional groups are confirmed by X-ray Photoelectron Spectroscopy (XPS). In correlation with the change of hydrodynamic size, PAA coated nanoparticles are found to exhibit outstanding stability in aqueous solution. Furthermore, we demonstrate that the functional groups are available for conjugating with other molecules such as fluorescent dye, showing potential biological applications. Lastly, the magnetic resonance phantom studies demonstrate that iron oxide nanoparticles with PAA coating can be used as T_1 and T_2 dual-modality contrast agents. Both r_1 and r_2 relaxivities significantly increase after surface functionalization with PAA, indicating improved sensitivity.

INTRODUCTION

Because of their unique magnetic property and excellent biocompatibility, iron oxide nanoparticles have tremendous potential applications in targeted drug delivery, bioseparation, magnetic resonance imaging (MRI), and cancer therapy. For these biomedical applications, the synthesis of iron oxide nanoparticles with controlled size and functional groups on the surface is essential. On one side, the size control of iron oxide nanoparticles is important because the magnetic properties are dependent on the size.[1,2] On the other side, the tailored surface coating can improve the colloidal stability, and the functional group on the surface can be used to conjugate bioactive molecules for targeted imaging and therapy.[3−5]

For the synthesis of monodispersed iron oxide nanoparticles, thermal decomposition has been a well-established method by decomposing iron precursors in organic solvents with high boiling points.[6−8] The size of the iron oxide nanoparticles can be controlled through the addition of alcohol, oleic acid, and oleylamine.[9] By seed-mediated growth, the size was precisely controlled from 6 to 12 nm.[2] However, the nanoparticles synthesized by thermal decomposition can only dissolve in organic solvents because the surface of nanoparticles is capped with hydrophobic ligands. A ligand exchange procedure is required to transfer the nanoparticles to an aqueous phase. The surface modification process is sophisticated and usually leads to a larger hydrodynamic size.[10−12] The poor colloidal stability in aqueous solution limits the biomedical application of iron oxide nanoparticles, especially in vivo applications. The surface

Received: November 17, 2020
Revised: December 31, 2020

https://dx.doi.org/10.1021/acs.langmuir.0c03314
Langmuir XXXX, XXX, XXX−XXX

modification is still a challenging task with a lot of research efforts still going on.

Polyols have emerged as an attractive method to synthesize nanoparticles, including iron oxide nanoparticles.[13,14] The typical polyols include ethylene glycol, diethylene glycol (DEG), triethylene glycol (TREG), and tetraethylene glycol (TEG). The advantages of polyols as solvents are high reaction temperatures and their solubility with both inorganic and organic reagents. Besides, the polyols act as both reducing agents and capping agents. The simplicity of the reaction makes it easy to scale up. Most importantly, the synthesized nanoparticles are water-soluble because the surface is coated with polyol molecules. It was much easier for the nanoparticles to be further functionalized for biomedical applications because the reaction is homogeneous.[3,15] However, a low level of size control was usually obtained compared with that from the thermal decomposition method in organic solvents. It was reported that the size was affected by reaction temperature and reaction time when $FeCl_3$ was used as a precursor.[16] The reaction conditions are largely empirical, and the size distribution is broad.[17]

Recently, we reported a continuous growth of iron oxide nanoparticles in polyols.[18] The size of iron oxide nanoparticles can be controlled precisely by the addition of precursors. Potentially, nanoparticles with nanometer-scale size increments can be achieved. The resultant nanoparticles exhibit extraordinarily high relaxivity and could potentially be used for high performance T_2 weighted contrast agents.

For advanced applications in biomedicine, further surface functionalization is highly desired. After the surface modification of nanoparticles, the targeting components can be conjugated on the surface to perform targeted imaging and therapy. In addition, the therapeutic drug can be loaded onto nanoparticles by its conjugation on the surface to increase efficacy and reduce toxicity.[19−21] There is an unmet need to prepare water dispersible iron oxide nanoparticles with precisely controlled size and surface functional groups.

In this study, we demonstrated a one-pot procedure to functionalize the surface of iron oxide nanoparticles immediately after the nanoparticles with different sizes are synthesized. Specifically, a continuous growth method is employed to synthesize monodispersed nanoparticles with precisely controlled size. After the nanoparticles with the desired size are synthesized, different coating materials are added immediately to prepare nanoparticles with various binding groups. Furthermore, we demonstrated that the functional groups are available for conjugating other molecules. Previous studies focused on surface coating during a reaction,[22,23] or post surface modification.[3,24] There is no report on the universal surface modification of iron oxide nanoparticles with tunable sizes in polyols. Besides, different surface functional groups can be obtained according to the needs. There is no need to change the synthetic conditions for different functional groups with nanoscale control on core size.

EXPERIMENTAL SECTION

Chemicals. Iron(III) acetylacetonate ($Fe(acac)_3$) ≥99.9%, diethylene glycols (DEG), dopamine hydrochloride (DOPA), poly(acrylic acid) (PAA) (Mw = 1,800), 1-ethyl-3-(3-dimethylaminoproply) carbodiimide (EDC), *N*-hydroxysuccinimide (NHS) were purchased from Sigma-Aldrich (St. Louis, USA). Polyethylene glycol (Mw = 5000) with thiol end group (thiol-PEG) was purchased from Laysan Bio Inc. (Alabama, USA), 5(6)-carboxy-X-rhodamine-N-succinimidylester (NHS-Rhodamine) was purchased from Fluka (Buchs, Switzerland). Ethylenediamine (EDA) was purchased from Fisher Chemical (New Jersey, USA). All chemicals were used without further purification, and Milli-Q water was used throughout this study.

Synthesis of Surface Functionalized-IO. The synthesis of iron oxide nanoparticles follows our previous study.[18] Typically, $Fe(acac)_3$ (88 mg, 0.25 mmol) was mixed and stirred with 2.5 mL of DEG (0.1 mmol Fe/ml) in a three-necked flask under argon gas exchange to obtain solution A. In another flask, $Fe(acac)_3$ (211 mg, 0.6 mmol) was mixed with 6 mL of DEG (0.1 mmol Fe/ml) and the mixture was stirred under argon to obtain solution B. Both solutions were heated to 120 °C for an hour. Solution B was kept at 70 °C for later use. Solution A was further heated to 220 °C for 2 h as the first growth. After that, solution B (2.5 mL, 0.25 mmol) was added subsequently to react for another 2 h. The addition of solution B continued until nanoparticles with the desired size were obtained. Prior to the end of the growth, surface ligands (0.3 to 1.5 mmol functional group) were prepared in 2 mL of DEG and dissolved at 70 °C. After the surface ligand mixture was then added, the reaction mixture was removed from the heat and stirred for 30 min as the mixture cooled down to room temperature. After being cooled to room temperature, the reaction mixture (50 μL) was mixed with 400 μL of Milli-Q water and the solution was purified by centrifugal filtration (Amicon, 30K) at 8000 rpm for 10 min. Milli-Q water was added to the centrifugal filter and centrifuged again. This process was repeated 3 times to get rid of excess surface ligands and DEG. The final products were dispersed in water, and the solution was stored at room temperature for future use. The purification step for IO-PAA was slightly different in which the reaction mixture (50 μL) was mixed with 400 μL of diluted sodium bicarbonate (0.15 wt %) and this mixture was purified by centrifugal filtration (Amicon, 30K) at 8000 rpm for 10 min. Diluted sodium bicarbonate (0.15 wt %) was added to the centrifugal filter and centrifuged again 2 times. Lastly, Milli-Q water was added and centrifuged for the third cycle to get rid of excess PAA and DEG.

Conjugation of Fluorescence Dyes to IO-PAA. NHS (5.8 mg, 0.05 mmol) and EDC (9.6 mg, 0.05 mmol) were mixed in 1 mL of water to make a NHS−EDC stock solution. Purified IO-PAA (0.001 mmol Fe) was dispersed in 0.9 mL of water, and to this mixture was added 0.1 mL of NHS−EDC stock. The mixture was shaken at 1000 rpm for 15 min. Ethylenediamine (EDA) (10 μL) was then added, and the mixture was shaken at 1000 rpm for 3 h. Next, the sample was purified by centrifugal filtration (Amicon, 30K) at 8000 rpm for 10 min. Milli-Q water was added to a centrifugal filter and centrifuged again for 3 cycles. NHS−Rhodamine (1.5 mg, 0.0025 mmol) was dissolved in 0.5 mL of water. NHS−Rhodamine dye (5 μL, 25 μmol) was added, and the sample was shaken at 1000 rpm for 3 h. Finally, the product was purified by centrifugal filtration (Amicon, 30K) at 8000 rpm for 10 min. Milli-Q water was added to the centrifugal filter and centrifuge again for 5 cycles.

Characterization. The core size of the nanoparticles was characterized by using a transmission electron microscope (TEM) JEOL JEM 1011. The dilute water dispersion of nanoparticles was cast on ultrathin 150-mesh carbon-coated grid and allowed to dry at room temperature. The size analysis from TEM images was performed using ImageJ software (Version 1.52a) by taking the average size of 100 particles. The statistics analysis was conducted in OriginPro 2018. The hydrodynamic size and ζ potential of nanoparticles in Milli-Q water were studied with dynamic light scattering (NanoZS, Malvern, Worcestershire, UK). The X-ray diffractograms were collected under a Rigaku MiniFlex 600 X-ray diffractometer (40 kV, 15 mA) using Cu Kβ radiation (λ = 0.154 nm). The scan degree is from 10° to 80°, step degree of 0.01 at the rate of 1° /min. The dried pellet was scanned using a Perkin Elmer Fourier transform infrared (FT-IR) spectrometer from 400 to 4000 cm^{-1} with a resolution of 4 cm^{-1} for 64 scans. Thermogravimetric analysis was used to determine the weight change of samples over the heating process. The analysis was performed using a TA Instruments Q500 TGA and Advantage for Q Series (Version 2.5.0.256, Thermal Advantage Release 5.5.22, TA Instruments-Waters LLC). The sample was freeze-dried prior to analysis. An adequate amount of sample was

https://dx.doi.org/10.1021/acs.langmuir.0c03314
Langmuir XXXX, XXX, XXX−XXX

Scheme 1. One-Pot Procedure to Synthesize Iron Oxide Nanoparticles with Controlled Sizes and Surface Functional Groups

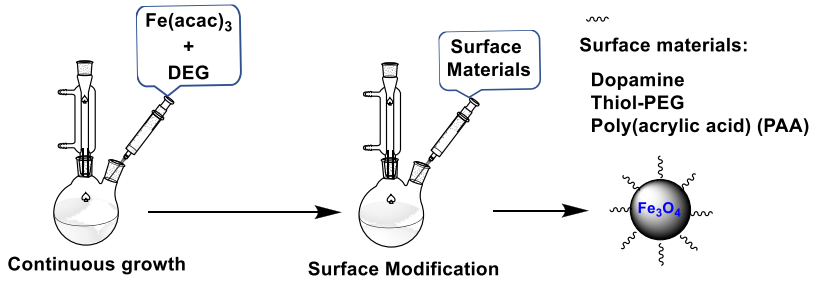

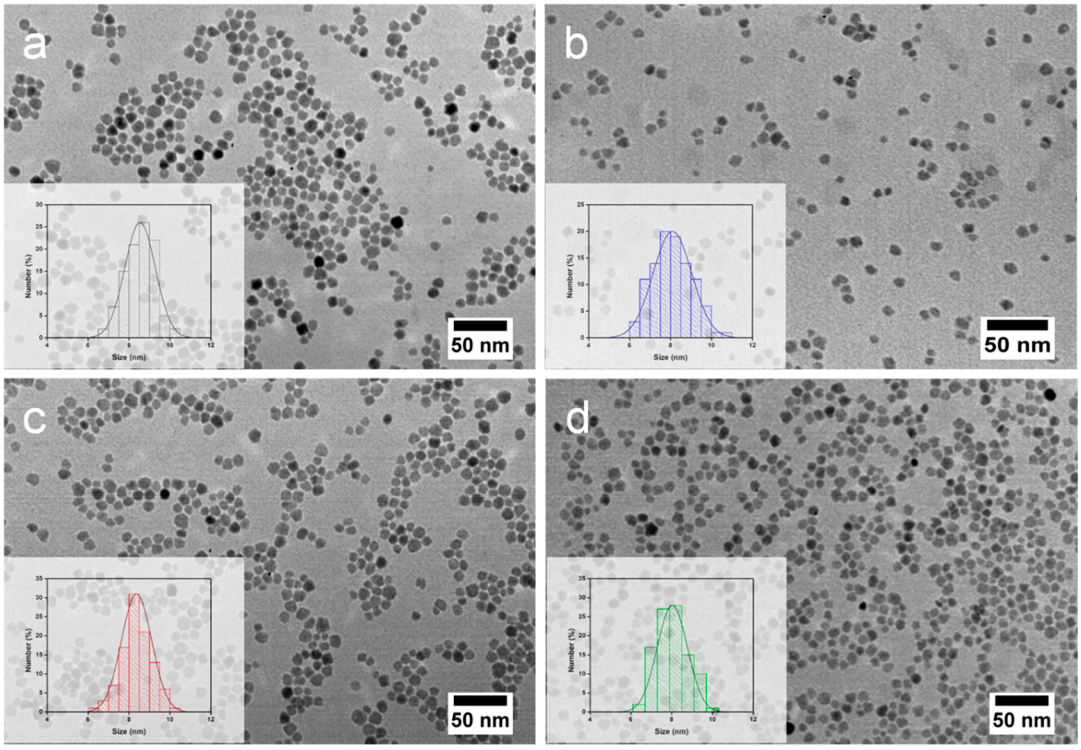

Figure 1. TEM images and nanoparticle size distribution histograms of (a) IO (8.5 ± 0.8 nm), (b) IO-DOPA (8.1 ± 0.9 nm), (c) IO-PEG (8.4 ± 0.7 nm), and (d) IO-PAA (8.0 ± 0.7 nm).

placed in a platinum pan and heated from 30 °C to 800 °C at 10 °C/min and 60 mL/min nitrogen gas flow. Data were analyzed using TA Universal Analysis (Version 4.5A, TA Instruments-Waters LLC). The density of surface ligands on the surface of iron oxide nanoparticles was according to the previous study.[18] After purified nanoparticles were dispersed in Milli-Q water or PBS buffer solution (1×), pictures were taken immediately and after 7 days to observe the stability. XPS was performed using a Thermo Fisher ESCALAB Xi+ spectrometer equipped with a monochromatic Al X-ray source (1486.6 eV). Measurements were performed using the standard magnetic lens mode and charge compensation. The base pressure in the analysis chamber during spectral acquisition was at 3×10^{-7} mbar. Spectra were collected at a takeoff angle of 90° from the plane of the surface. The pass energy of the analyzer was set at 150 eV for survey scans with an energy resolution of 1.0 eV; the total acquisition time was 220 s. Binding energies were calibrated with respect to C 1s at 284.8 eV. All spectra were recorded using the Thermo Scientific Avantage software; data files were translated to VGD format and processed using the Thermo Avantage package v5.9904. T_1 and T_2 relaxation times of a series of nanoparticles dispersion with different iron concentrations were measured with Niumag 0.5 T relaxometer at 32 °C. NMR Analyzing Software Ver. 4.0 was used to compute for T_1 and T_2. The specific relaxivities of r_1 and r_2 for each nanoparticle were computed by taking the linear slope of $1/T_i$ versus Fe concentration. T_1 and T_2 images for each nanoparticle at different iron concentrations were collected with NMR Imaging Software. The iron concentration was analyzed with an inductively coupled plasma mass spectrometer (ICP-MS) (Varian 820).

RESULTS AND DISCUSSION

Surface Functionalization of Iron Oxide Nanoparticles with Various Ligands. The iron oxide nanoparticles were synthesized at elevated temperatures in DEG.[18] The size can be controlled by sequentially adding the $Fe(acac)_3$ precursor. The iron oxide nanoparticles have very good size control and great dispersibility in water. In order to produce more versatile functionality for advanced application, we further added surface ligand molecules at the end of the reaction via a one-pot reaction. Due to the amphiphilic property of DEG, the surface modification take place in a homogeneous solution which make the process efficient. The overall procedure is illustrated in Scheme 1. As a comparison, different surface materials, i.e., DOPA, thiol-PEG, and PAA, are studied. The chemical structure of each surface ligand is shown in Table S1.

https://dx.doi.org/10.1021/acs.langmuir.0c03314
Langmuir XXXX, XXX, XXX−XXX

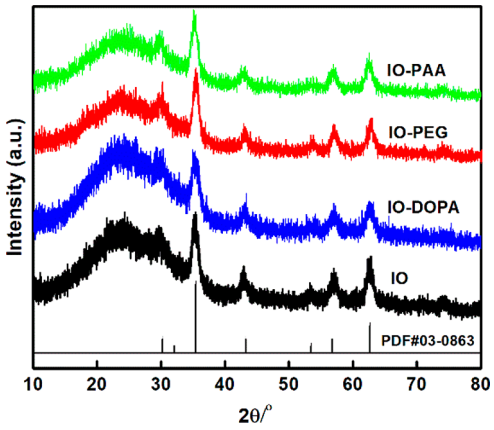

Figure 2. XRD patterns of IO, IO-DOPA, IO-PEG, and IO-PAA.

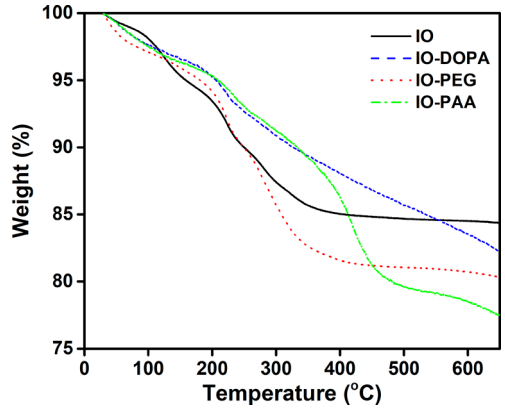

Figure 4. Thermogravimetric analysis of IO, IO-DOPA, IO-PEG, and IO-PAA, showing weight percent (%) as a function of temperature (°C).

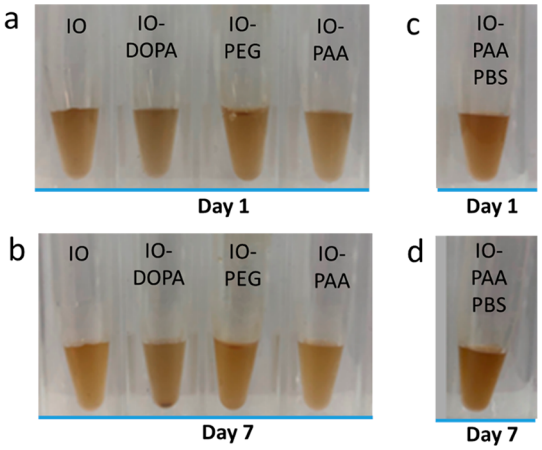

Figure 5. Photographs of nanoparticles dispersion: IO, IO-DOPA, IO-PEG, and IO-PAA in the water (a) before and (b) after 7 days; IO-PAA in 1 × PBS buffer solution (c) before (d) after 7 days.

During the surface modification, the morphology of nanoparticles is studied by TEM (Figure 1). For iron oxide nanoparticles with a core size of 8 nm, there are no obvious changes in the morphology before and after surface modifications. The size distributions remain narrow after surface modifications. As shown in Table S2, the sizes of iron oxide nanoparticles without surface modification (note as IO) are calculated to be 8.5 ± 0.8, and 8.1 ± 0.9, 8.4 ± 0.7, and 8.0 ± 0.7 for nanoparticles modified with DOPA (IO-DOPA), thiol-PEG (IO-PEG), and PAA (IO-PAA), respectively. The results indicated that surface ligands have no effect on the nanoparticles core during surface modification.

The surface ligands consisting of different functional groups have different effects on the hydrodynamic sizes and their corresponding surface charges. The dynamic light scattering (DLS) curves exhibit a single peak for all nanoparticles (Figure S1). As shown in Table S2, the IO and IO-PEG have very similar hydrodynamic (HD) sizes (~14 nm), while that of IO-PAA is slightly higher (~18 nm). The IO-DOPA has the largest HD size (~46 nm). The iron oxide nanoparticles before surface modification with remaining DEG on the surface have a positive surface charge (+ 46 mV). The DOPA binds onto positively charged iron oxide nanoparticles via the catechol group,[25] and the positive-charged end group ($-NH_3^+$) rendered IO-DOPA with positive surface charge (+40 mV). When coated with thiol-PEG, the binding of thiol-ligands to iron oxide nanoparticles is weaker than that of the catechol-derivative group.[26] The smaller binding of thiol-Fe may result in a little increase of HD size and only a slight reduction of surface charge (+34 mV). Meanwhile, PAA binds strongly to iron oxide nanoparticles via the carboxyl end group[27,28] and gives a highly negative surface charge (−48 mV) due to the abundance of carboxylate ions ($-COO^-$) repeating unit from the PAA polymer chain. These results indicated the successful binding of different surface ligands on iron oxide nanoparticles.

X-ray diffraction was also used to study the crystalline phase of these nanoparticles (Figure 2). The patterns show a similar structure as the standard bulk phase for magnetite Fe_3O_4 (JCPDS no. 03−0863), and there is no change in the crystalline phase after the surface modifications.

Surface Functional Group. From the FTIR characterization, we obtained detailed information on the surface ligand binding to the nanoparticles (Figure 3). The iron oxide

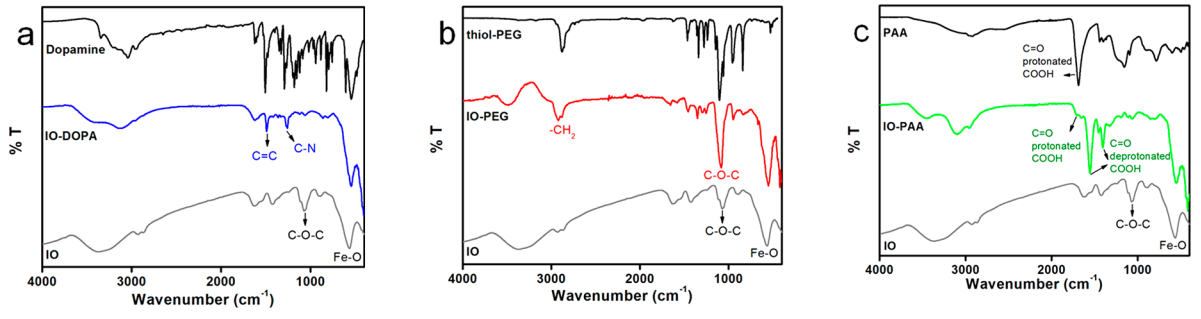

Figure 3. FTIR spectra of (a) IO-DOPA, (b) IO-PEG, and (c) IO-PAA, compared to IO and its corresponding surface ligand.

https://dx.doi.org/10.1021/acs.langmuir.0c03314
Langmuir XXXX, XXX, XXX−XXX

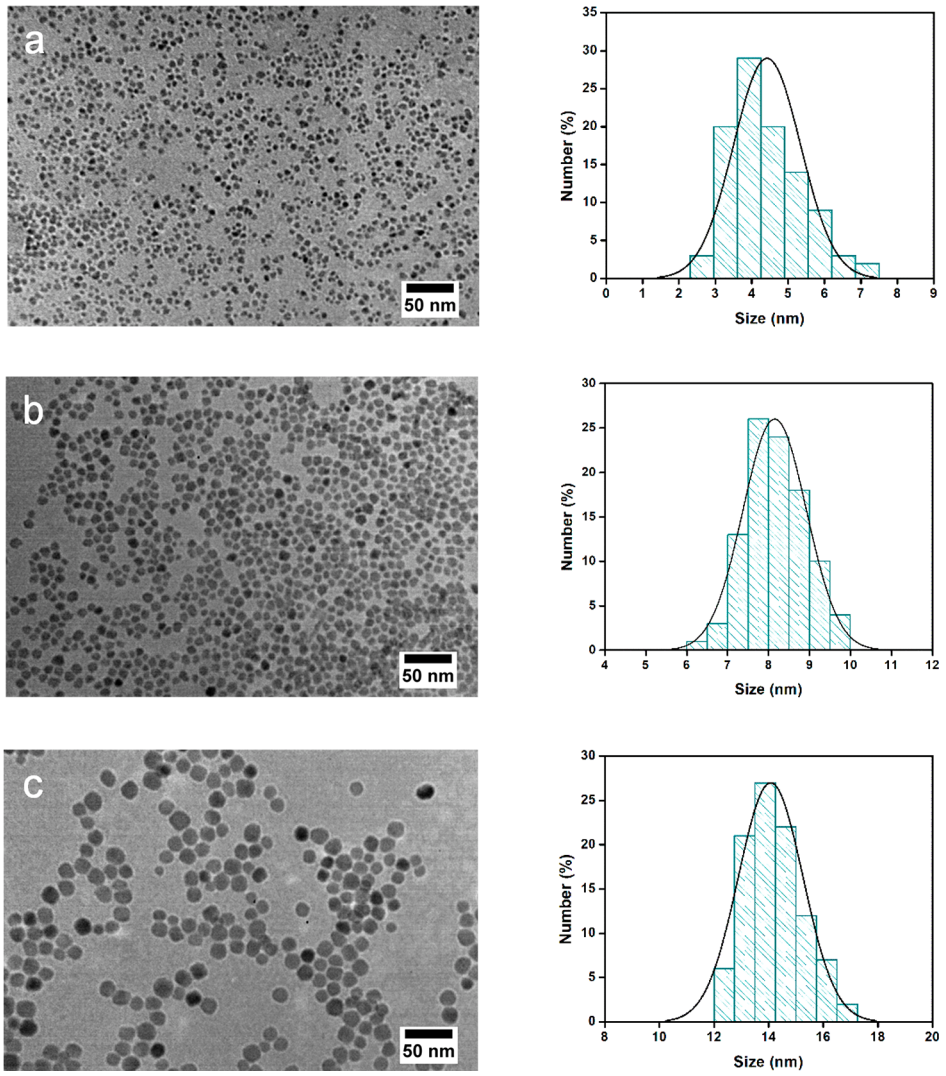

Figure 6. TEM images and nanoparticle size distribution histogram of iron oxide nanoparticles coated with PAA at increment size: (a) 4.4 ± 0.9 nm, (b) 8.1 ± 0.8 nm, and (c) 14.1 ± 1.2 nm.

nanoparticles before surface modification have the characteristic peaks of 1057 and 2921 cm^{-1} attributed to the C−O and CH_2 vibrations of DEG.[29,30] The broad absorption centered around 3500 cm^{-1} is from the stretching vibration of O−H from both DEG and absorbed water. The characteristic peak at 531 cm^{-1} for Fe−O stretching indicates that iron oxide nanoparticles are Fe_3O_4.[31] The IO-DOPA shows the characteristic peak of dopamine with aromatics C−H, C=C, and C−N stretching at 3109, 1490, and 1270 cm^{-1}, respectively (Figure 3a). The IO-PEG showed C−O−C stretching of thiol-PEG at around 1083 cm^{-1}.[29] Although this characteristic peak of C−O−C overlaps with the DEG due to the similar functional group, the intensity of the peak increases in IO-PEG (Figure 3b). The IO-PAA shows the presence of PAA on the surface of IO with characteristics bands for $-CH_2$ bending. The asymmetric and symmetric C−O stretching at 1553 and 1404 cm^{-1} correspond to the deprotonated carboxylate group (COO^-).[23] This is slightly shifted when compared with that of the sharp peak at 1700 cm^{-1} of the protonated carboxylate group (COOH) in pure PAA (Figure 3c).

We also studied the thermogravimetric analysis of these samples in order to confirm the ligand exchange on the surface of the iron oxide nanoparticles. A total weight loss over increasing temperature is 15.5%, 16.4%, 19.3%, and 21.6% for IO, IO-DOPA, IO-PEG, and IO-PAA, respectively (Figure 4). All nanoparticles after being coated with surface ligands have a higher weight loss than that of iron oxide nanoparticles, indicating the presence of surface materials on the surface. Assuming all DEG molecules on the surface were replaced by the surface ligands upon surface functionalization, we estimated the surface coverage of each corresponding surface ligand on the iron oxide nanoparticles. The surface coverage follows the order of thiol-PEG < PAA < DOPA with 0.18 thiol-PEG molecules, 0.67 PAA molecules, and 3.3 DOPA molecules attached on every nm^2 of nanoparticles (Table S3). This result agrees with the trend observed in HD size change. Davis et al. quantitatively studied the ligand exchange between different PEG ligands and radiolabeled oleic acid coated iron oxide nanoparticles using both TGA and liquid scintillation counting (LSC) results.[32] They reported the coverage densities of each PEG ligands in the increasing order of PEG-COOH < PEG-NH_2≪ PEG-nitro DOPA≪ PEG-phosphonate ≪ PEG-DOPA. The surface ligand with a catechol derived anchor group (i.e., DOPA) indeed binds strongly onto iron oxide nanoparticles as observed in our TGA results.

https://dx.doi.org/10.1021/acs.langmuir.0c03314
Langmuir XXXX, XXX, XXX−XXX

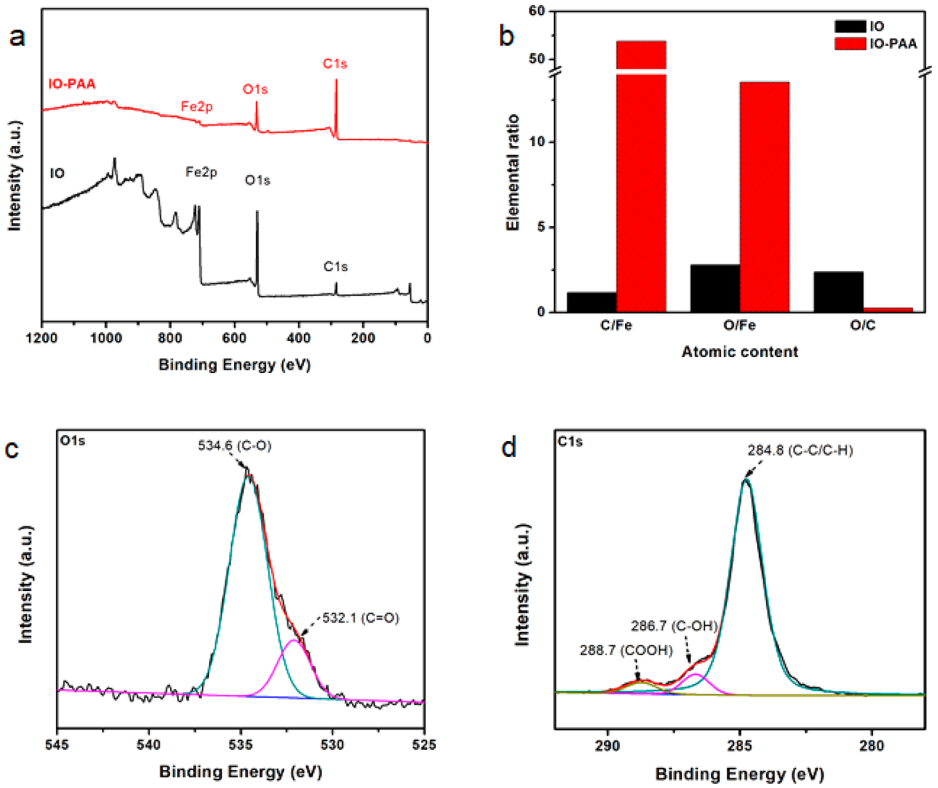

Figure 7. XPS spectra, (a) wide scan and (b) C/Fe, O/Fe, and O/C elemental ratios for IO and IO-PAA; (c) O 1s, and (d) C 1s for IO-PAA.

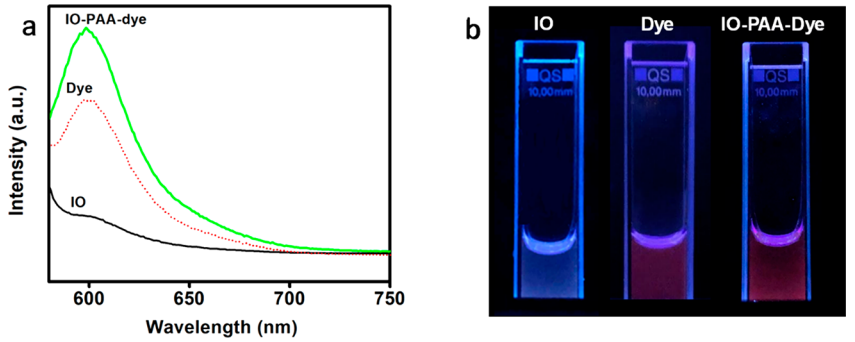

Figure 8. (a) Emission spectra at excitation λ_{Ex} 550 nm and (b) the corresponding fluorescence images under UV lamp (λ= 365 nm) before and after conjugation of Rhodamine dye.

Stability in Water and Buffer Solution. All surface functionalized nanoparticles exhibited great dispersibility in water. As shown in Figure 5, surface-functionalized nanoparticles were stable in water after at least 1 week, except for IO-DOPA which showed slight precipitation (Figure 5a,b). The IO-DOPA tends to aggregate, which can be evidenced by the relatively high HD size mentioned previously. A possible reason is that dopamine induced the degradation of magnetite iron oxide nanoparticles when reacted with the oxygen on the surface of nanoparticles to form insoluble iron(III) oxyhydroxide.[33] Among all the surface functionalized nanoparticles, IO-PAA showed excellent stability in both water and phosphate buffer saline (1× PBS) after a week (Figure 5c,d). The high water dispersibility of these nanoparticles also implied the advantage of the homogeneous ligand exchange reaction in our synthesis method. Next, we will further study surface coating with PAA.

Surface Coating of Iron Oxide Nanoparticles with Different Sizes. The advantage of this study is that the sizes of iron oxide nanoparticles can be precisely controlled. Utilizing this facile one-pot synthesis and surface functionalization, we demonstrated the ability to modify the surfaces of the iron oxide nanoparticles with different sizes. The size of the nanoparticles is first controlled by the continuous addition of the starting materials; then the surface coating materials are added after the desired size was synthesized. The TEM images of the nanoparticles with sizes are shown in Figure 6. Nanoparticles with incremental sizes of 4.4, 8.1, and 14.1 nm can be obtained. Meanwhile, the size distribution is narrow for all sizes.

XPS before and after the Functionalization of PAA. We further studied the surface composition of IO-PAA by XPS (Figure 7). The wide scan XPS spectra for iron oxide nanoparticles before and after PAA coating are shown in Figure 7a. The XPS signals for iron oxide nanoparticles before

https://dx.doi.org/10.1021/acs.langmuir.0c03314
Langmuir XXXX, XXX, XXX−XXX

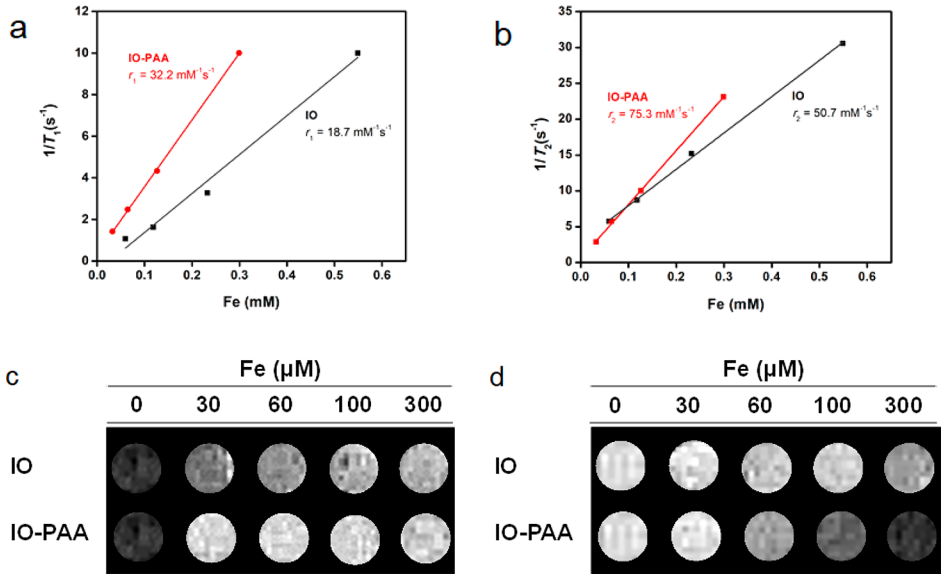

Figure 9. Magnetic resonance imaging relaxivity and phantom study of 8 nm iron oxide nanoparticles before and after surface functionalized with PAA under 0.5 T: (a) The inverse of the T_1 weighted and (b) T_2 weighted relaxation times as the function of iron concentrations; (c) T_1 weighted and (d) T_2 weighted MR phantom images.

coating are dominated by the iron oxide cores (Fe and O), while the signals for IO-PAA are dominated by the organic component (C and O) stoichiometrically (Table S4). The remarkable increase in the elemental ratios of C/Fe and O/Fe after surface functionalization confirms the successful coating of PAA on the surface of the iron oxide nanoparticles (Figure 7b). Meanwhile, the ratio for O/C greatly decreases in IO-PAA due to the increase of carbon concentration from the coated PAA. The peak deconvolution of Fe 2p for IO-PAA shows a relatively low signal of Fe 2p1/2 and Fe 2p3/2 due to a high concentration of organic surface ligands (Figure S2). High resolution O 1s spectrum in Figure 7c can be fitted into a monodentate oxygen moiety (C−O) at 534.6 eV and a bidentate carboxylate moiety (C=O) at 532.1 eV.[34] Fitting for the C 1s spectrum in Figure 7d shows aliphatic C−C/C−H, carboxylic O−C=O, and alcohol C−OH at 284.8, 288.7, and 286.7 eV, respectively.[34,35] Both O 1s and C 1s spectra indicate the presence of carboxylate groups on the surface of IO-PAA.

Potential for Further Bioconjugation. To evaluate the availability of functional groups on the surface functionalized iron oxide nanoparticles, we specifically utilized −COOH functional groups to conjugate fluorescent dye covalently. The IO-PAA with the − COOH end group was first activated with EDC and NHS and then reacted with EDA to obtain the amine end group before being coupled with NHS-Rhodamine. The overall procedure is shown in Scheme S1. After purification, the emission spectra at λ_{Ex} = 550 nm showed that rhodamine was successfully conjugated onto iron oxide nanoparticles (Figure 8a). In addition, rhodamine conjugated nanoparticles display a red fluorescence under a UV lamp (λ = 365 nm) (Figure 8b). The results confirmed the availability of the carboxylic acid groups on the surface of the iron oxide nanoparticles.[33] The conjugation of the fluorescent molecules onto the iron oxide nanoparticles demonstrates the capability of further bioconjugation for advanced applications when targeted imaging and therapy are needed.[3,15,36−39]

Values of r_1 and r_2 before and after the Functionalization of PAA. Longitudinal relaxivity (r_1) and transverse relaxivity (r_2) are important parameters to determine the efficiency of a T_1 or T_2 weighted contrast agent. To evaluate the efficiency of iron oxide nanoparticles before and after surface functionalization of PAA, we studied relaxation times using a benchtop relaxiometer at 0.5 T. The inverse of relaxation times ($1/T_i$) is plotted against different iron concentrations, and the relaxivities (r_i) are calculated from the slope (Figure 9a,b). The r_2, r_1, and the r_2/r_1 ratio are summarized in Table S5. The increase of r_1 and r_2 after the functionalization of PAA indicated that the sensitivity was greatly improved. This is attributed to the presence of hydrophilic PAA layers on the surface of magnetic nanoparticles, causing an increased volume of slow diffusion water around the nanoparticles and hence shortening the dephasing time for water proton spinning under an applied magnetic field, as explained by the modeling approaches of La Conte's work.[40] Our finding is in line with other previous studies that reported the increase of r_1 and r_2 with the increasing hydrophilic layer on the surface of nanoparticles.[4,24,41−43] In this study, we observe that r_1 has a steeper slope change (1.7×) after the surface functionalization of PAA at the same core and HD size. This increase of r_1 is well correlated with the enhanced hydrophilicity and dispersibility of IO-PAA in water and saline shown in the earlier section. The great r_1 in the presence of the PAA coating indicates the possibility of designing a T_1 weighted contrast agent with a larger core size (>5 nm) by optimization of the surface chemistry. In theory, r_1 is greatly affected by the surface chemistry involving the chemical exchange between water and paramagnetic ions (unpaired electrons) on the iron oxide nanoparticle surface. Meanwhile, r_2 depends on the magnetic spin in the nanocrystals structure as well as the surface chemistry change.[44] In order to demonstrate the effectiveness in MRI contrast, T_1 and T_2 weighted imaging for iron oxide nanoparticles and IO-PAA was shown in Figure 9c,d. With an increase in iron concentration, there is enhancement of the brighten signal on the T_1 weighted MR imaging (Figure 9c) and a darken signal on the T_2 weighted MR imaging (Figure 9d). The results show that IO-PAA can be used as a contrast agent for both T_1 (brighten) and T_2 (darken).

https://dx.doi.org/10.1021/acs.langmuir.0c03314
Langmuir XXXX, XXX, XXX−XXX

CONCLUSIONS

In this work, we described a versatile method to prepare water-soluble monodispersal iron oxide nanoparticles with various surface materials. The iron oxide nanoparticles were first synthesized by the thermal decomposition of $Fe(acac)_3$ in diethylene glycol (DEG), and their surfaces were modified by addition of the surface ligands at the end of the reaction. The size of the iron oxide nanoparticles was precisely controlled from 4 to 14 nm by continuous growth. The TEM study showed no changes in the core size and morphology of nanoparticles before and after surface functionalization. The surface chemistry of these iron oxide nanoparticles was studied using FTIR, TGA, and XPS, confirming the effectiveness of surface modification. From the DLS study, IO-PEG and IO-PAA displayed a slight increase in HD size while IO-DOPA displayed a large HD size. All surface functionalized nanoparticles exhibited great dispersibility in water. Particularly, the IO-PAA showed the most promising performance with narrow size distribution and high stability in water and saline solution which is desired for biological application. Moreover, as shown by the covalent coupling with fluorescent molecules, the abundance of functional groups on the surface of iron oxide nanoparticles enabled further bioconjugation for advanced applications. Finally, the magnetic resonance phantom study showed that the relaxivities of the iron oxide nanoparticles increased after being coated with PAA, indicating improved sensitivity. The resultant nanoparticles can be used as T_1 and T_2 dual-modality contrast agents with r_2/r_1= 2.34 at 0.5 T.

ASSOCIATED CONTENT

Supporting Information

The Supporting Information is available free of charge at https://pubs.acs.org/doi/10.1021/acs.langmuir.0c03314.

Structures of surface materials, DLS plot, surface coverage, XPS elemental composition, and dye coupling reaction scheme (PDF)

AUTHOR INFORMATION

Corresponding Author

Yongfeng Zhao − *Department of Chemistry, Physics, and Atmospheric Science, Jackson State University, Jackson, Mississippi 39217, United States;* orcid.org/0000-0003-2962-7504; Email: yongfeng.zhao@jsums.edu

Authors

Pohlee Cheah − *Department of Chemistry, Physics, and Atmospheric Science, Jackson State University, Jackson, Mississippi 39217, United States*

Paul Brown − *Department of Chemistry, Physics, and Atmospheric Science, Jackson State University, Jackson, Mississippi 39217, United States*

Jing Qu − *Department of Chemistry, Physics, and Atmospheric Science, Jackson State University, Jackson, Mississippi 39217, United States*

Bin Tian − *Department of Chemistry, Physics, and Atmospheric Science, Jackson State University, Jackson, Mississippi 39217, United States*

Derek L. Patton − *School of Polymer Science and Engineering, University of Southern Mississippi, Hattiesburg, Mississippi 39406, United States;* orcid.org/0000-0002-8738-4750

Complete contact information is available at: https://pubs.acs.org/10.1021/acs.langmuir.0c03314

Notes

The authors declare no competing financial interest.

ACKNOWLEDGMENTS

This research was supported by the National Science Foundation (grant number: HRD-1700390, DMR-2000135) and NSF EPSCoR (grant number: OIA-1757220). We thank Ryan Dufrene for the help with TGA measurement.

REFERENCES

(1) Lee, J.-H.; Huh, Y.-M.; Jun, Y.-w.; Seo, J.-w.; Jang, J.-T.; Song, H.-T.; Kim, S.; Cho, E.-J.; Yoon, H.-G.; Suh, J.-S.; Cheon, J. Artificially engineered magnetic nanoparticles for ultra-sensitive molecular imaging. *Nat. Med.* **2007**, *13*, 95−99.

(2) Park, J.; Lee, E.; Hwang, N.-M.; Kang, M.; Kim, S. C.; Hwang, Y.; Park, J.-G.; Noh, H.-J.; Kim, J.-Y.; Park, J.-H.; Hyeon, T. One-Nanometer-Scale Size-Controlled Synthesis of Monodisperse Magnetic Iron Oxide Nanoparticles. *Angew. Chem., Int. Ed.* **2005**, *44*, 2872−2877.

(3) Qu, H.; Caruntu, D.; Liu, H.; O'Connor, C. J. Water-Dispersible Iron Oxide Magnetic Nanoparticles with Versatile Surface Functionalities. *Langmuir* **2011**, *27*, 2271−2278.

(4) Tong, S.; Hou, S.; Zheng, Z.; Zhou, J.; Bao, G. Coating Optimization of Superparamagnetic Iron Oxide Nanoparticles for High T2 Relaxivity. *Nano Lett.* **2010**, *10*, 4607−4613.

(5) Huang, G.; Zhang, C.; Li, S.; Khemtong, C.; Yang, S.-G.; Tian, R.; Minna, J. D.; Brown, K. C.; Gao, J. A novel strategy for surface modification of superparamagnetic iron oxide nanoparticles for lung cancer imaging. *J. Mater. Chem.* **2009**, *19*, 6367−6372.

(6) Kim, B. H.; Lee, N.; Kim, H.; An, K.; Park, Y. I.; Choi, Y.; Shin, K.; Lee, Y.; Kwon, S. G.; Na, H. B.; Park, J.-G.; Ahn, T.-Y.; Kim, Y.-W.; Moon, W. K.; Choi, S. H.; Hyeon, T. Large-Scale Synthesis of Uniform and Extremely Small-Sized Iron Oxide Nanoparticles for High-Resolution T1Magnetic Resonance Imaging Contrast Agents. *J. Am. Chem. Soc.* **2011**, *133*, 12624−12631.

(7) Park, J.; An, K.; Hwang, Y.; Park, J.-G.; Noh, H.-J.; Kim, J.-Y.; Park, J.-H.; Hwang, N.-M.; Hyeon, T. Ultra-large-scale syntheses of monodisperse nanocrystals. *Nat. Mater.* **2004**, *3*, 891−895.

(8) Sun, S.; Zeng, H.; Robinson, D. B.; Raoux, S.; Rice, P. M.; Wang, S. X.; Li, G. Monodisperse MFe2O4 (M = Fe, Co, Mn) Nanoparticles. *J. Am. Chem. Soc.* **2004**, *126*, 273−279.

(9) Sun, S.; Zeng, H. Size-Controlled Synthesis of Magnetite Nanoparticles. *J. Am. Chem. Soc.* **2002**, *124*, 8204−8205.

(10) Wang, W.; Ji, X.; Na, H. B.; Safi, M.; Smith, A.; Palui, G.; Perez, J. M.; Mattoussi, H. Design of a Multi-Dopamine-Modified Polymer Ligand Optimally Suited for Interfacing Magnetic Nanoparticles with Biological Systems. *Langmuir* **2014**, *30*, 6197−6208.

(11) Huang, J.; Wang, L.; Zhong, X.; Li, Y.; Yang, L.; Mao, H. Facile non-hydrothermal synthesis of oligosaccharide coated sub-5 nm magnetic iron oxide nanoparticles with dual MRI contrast enhancement effects. *J. Mater. Chem. B* **2014**, *2*, 5344−5351.

(12) Xie, J.; Xu, C.; Kohler, N.; Hou, Y.; Sun, S. Controlled PEGylation of Monodisperse Fe3O4 Nanoparticles for Reduced Non-Specific Uptake by Macrophage Cells. *Adv. Mater.* **2007**, *19*, 3163−3166.

(13) Dong, H.; Chen, Y. C.; Feldmann, C. Polyol synthesis of nanoparticles: status and options regarding metals, oxides, chalcogenides, and non-metal elements. *Green Chem.* **2015**, *17*, 4107−4132.

(14) Fiévet, F.; Ammar-Merah, S.; Brayner, R.; Chau, F.; Giraud, M.; Mammeri, F.; Peron, J.; Piquemal, J. Y.; Sicard, L.; Viau, G. The polyol process: a unique method for easy access to metal nanoparticles with tailored sizes, shapes and compositions. *Chem. Soc. Rev.* **2018**, *47*, 5187−5233.

(15) Miguel-Sancho, N.; Bomatí-Miguel, O.; Colom, G.; Salvador, J. P.; Marco, M. P.; Santamaría, J. Development of Stable, Water-Dispersible, and Biofunctionalizable Superparamagnetic Iron Oxide Nanoparticles. *Chem. Mater.* **2011**, *23*, 2795−2802.

(16) Shen, L.-h.; Bao, J.-f.; Wang, D.; Wang, Y.-x.; Chen, Z.-w.; Ren, L.; Zhou, X.; Ke, X.-b.; Chen, M.; Yang, A.-q. One-step synthesis of monodisperse, water-soluble ultra-small Fe3O4 nanoparticles for potential bio-application. *Nanoscale* **2013**, *5*, 2133−2141.
(17) Hachani, R.; Lowdell, M.; Birchall, M.; Hervault, A.; Mertz, D.; Begin-Colin, S.; Thanh, N. T. K. Polyol synthesis, functionalisation, and biocompatibility studies of superparamagnetic iron oxide nanoparticles as potential MRI contrast agents. *Nanoscale* **2016**, *8*, 3278−3287.
(18) Cheah, P.; Cowan, T.; Zhang, R.; Fatemi-Ardekani, A.; Liu, Y.; Zheng, J.; Han, F.; Li, Y.; Cao, D.; Zhao, Y. Continuous growth phenomenon for direct synthesis of monodisperse water-soluble iron oxide nanoparticles with extraordinarily high relaxivity. *Nanoscale* **2020**, *12*, 9272−9283.
(19) Thiruppathi, R.; Mishra, S.; Ganapathy, M.; Padmanabhan, P.; Gulyás, B. Nanoparticle Functionalization and Its Potentials for Molecular Imaging. *Advanced Science* **2017**, *4*, 1600279.
(20) Goodman, C. M.; McCusker, C. D.; Yilmaz, T.; Rotello, V. M. Toxicity of Gold Nanoparticles Functionalized with Cationic and Anionic Side Chains. *Bioconjugate Chem.* **2004**, *15*, 897−900.
(21) Montes-Fonseca, S. L.; Orrantia-Borunda, E.; Aguilar-Elguezabal, A.; González Horta, C.; Talamás-Rohana, P.; Sánchez-Ramírez, B. Cytotoxicity of functionalized carbon nanotubes in J774A macrophages. *Nanomedicine* **2012**, *8*, 853−859.
(22) Dai, L.; Liu, Y.; Wang, Z.; Guo, F.; Shi, D.; Zhang, B. One-pot facile synthesis of PEGylated superparamagnetic iron oxide nanoparticles for MRI contrast enhancement. *Mater. Sci. Eng., C* **2014**, *41*, 161−167.
(23) Ge, J.; Hu, Y.; Biasini, M.; Dong, C.; Guo, J.; Beyermann, W. P.; Yin, Y. One-Step Synthesis of Highly Water-Soluble Magnetite Colloidal Nanocrystals. *Chem. - Eur. J.* **2007**, *13*, 7153−7161.
(24) Hu, F.; MacRenaris, K. W.; Waters, E. A.; Liang, T.; Schultz-Sikma, E. A.; Eckermann, A. L.; Meade, T. J. Ultrasmall, Water-Soluble Magnetite Nanoparticles with High Relaxivity for Magnetic Resonance Imaging. *J. Phys. Chem. C* **2009**, *113*, 20855−20860.
(25) Amstad, E.; Gillich, T.; Bilecka, I.; Textor, M.; Reimhult, E. Ultrastable Iron Oxide Nanoparticle Colloidal Suspensions Using Dispersants with Catechol-Derived Anchor Groups. *Nano Lett.* **2009**, *9*, 4042−4048.
(26) Davis, K.; Cole, B.; Ghelardini, M.; Powell, B. A.; Mefford, O. T. Quantitative Measurement of Ligand Exchange with Small-Molecule Ligands on Iron Oxide Nanoparticles via Radioanalytical Techniques. *Langmuir* **2016**, *32*, 13716−13727.
(27) Zhang, T.; Ge, J.; Hu, Y.; Yin, Y. A General Approach for Transferring Hydrophobic Nanocrystals into Water. *Nano Lett.* **2007**, *7*, 3203−3207.
(28) Palchoudhury, S.; Xu, Y.; An, W.; Turner, C. H.; Bao, Y. Platinum attachments on iron oxide nanoparticle surfaces. *J. Appl. Phys.* **2010**, *107*, 09B311.
(29) Larkin, P.: Chapter 8 - Illustrated IR and Raman Spectra Demonstrating Important Functional Groups. In *Infrared and Raman Spectroscopy*; Larkin, P., Ed.; Elsevier: Oxford, 2011; pp 135−176.
(30) Khoee, S.; Kavand, A. A new procedure for preparation of polyethylene glycol-grafted magnetic iron oxide nanoparticles. *Journal of Nanostructure in Chemistry* **2014**, *4*, 111.
(31) Cornell, R. M.; Schwertmann, U. *Characterization. In In The Iron Oxides* **2003**, 139−183.
(32) Davis, K.; Qi, B.; Witmer, M.; Kitchens, C. L.; Powell, B. A.; Mefford, O. T. Quantitative Measurement of Ligand Exchange on Iron Oxides via Radiolabeled Oleic Acid. *Langmuir* **2014**, *30*, 10918−10925.
(33) Shultz, M. D.; Reveles, J. U.; Khanna, S. N.; Carpenter, E. E. Reactive Nature of Dopamine as a Surface Functionalization Agent in Iron Oxide Nanoparticles. *J. Am. Chem. Soc.* **2007**, *129*, 2482−2487.
(34) Louette, P.; Bodino, F.; Pireaux, J.-J. Poly(acrylic acid) (PAA) XPS Reference Core Level and Energy Loss Spectra. *Surf. Sci. Spectra* **2005**, *12*, 22−26.
(35) Kolen'ko, Y. V.; Bañobre-López, M.; Rodríguez-Abreu, C.; Carbó-Argibay, E.; Sailsman, A.; Piñeiro-Redondo, Y.; Cerqueira, M. F.; Petrovykh, D. Y.; Kovnir, K.; Lebedev, O. I.; Rivas, J. Large-Scale Synthesis of Colloidal Fe3O4 Nanoparticles Exhibiting High Heating Efficiency in Magnetic Hyperthermia. *J. Phys. Chem. C* **2014**, *118*, 8691−8701.
(36) Xie, J.; Peng, S.; Brower, N.; Pourmand, N.; Wang, S. X.; Sun, S. One-pot synthesis of monodisperse iron oxide nanoparticles for potential biomedical applications. *Pure Appl. Chem.* **2006**, *78*, 1003.
(37) Yin, T.; Huang, P.; Gao, G.; Shapter, J. G.; Shen, Y.; Sun, R.; Yue, C.; Zhang, C.; Liu, Y.; Zhou, S.; Cui, D. Superparamagnetic Fe3O4-PEG2K-FA@Ce6 Nanoprobes for in Vivo Dual-mode Imaging and Targeted Photodynamic Therapy. *Sci. Rep.* **2016**, *6*, 36187.
(38) Lin, L.-S.; Cong, Z.-X.; Cao, J.-B.; Ke, K.-M.; Peng, Q.-L.; Gao, J.; Yang, H.-H.; Liu, G.; Chen, X. Multifunctional Fe3O4@ Polydopamine Core−Shell Nanocomposites for Intracellular mRNA Detection and Imaging-Guided Photothermal Therapy. *ACS Nano* **2014**, *8*, 3876−3883.
(39) Yen, S. K.; Padmanabhan, P.; Selvan, S. T. Multifunctional Iron Oxide Nanoparticles for Diagnostics, Therapy and Macromolecule Delivery. *Theranostics* **2013**, *3*, 986−1003.
(40) LaConte, L. E. W.; Nitin, N.; Zurkiya, O.; Caruntu, D.; O'Connor, C. J.; Hu, X.; Bao, G. Coating thickness of magnetic iron oxide nanoparticles affects R2 relaxivity. *Journal of Magnetic Resonance Imaging* **2007**, *26*, 1634−1641.
(41) Pellico, J.; Ruiz-Cabello, J.; Fernández-Barahona, I.; Gutiérrez, L.; Lechuga-Vieco, A. V.; Enríquez, J. A.; Morales, M. P.; Herranz, F. One-Step Fast Synthesis of Nanoparticles for MRI: Coating Chemistry as the Key Variable Determining Positive or Negative Contrast. *Langmuir* **2017**, *33*, 10239−10247.
(42) Meisel, C. L.; Bainbridge, P.; Mulkern, R. V.; Mitsouras, D.; Wong, J. Y. Assessment of Superparamagnetic Iron Oxide Nanoparticle Poly(Ethylene Glycol) Coatings on Magnetic Resonance Relaxation for Early Disease Detection. *IEEE Open Journal of Engineering in Medicine and Biology* **2020**, *1*, 116−122.
(43) Guleria, A.; Pranjali, P.; Meher, M. K.; Chaturvedi, A.; Chakraborti, S.; Raj, R.; Poluri, K. M.; Kumar, D. Effect of Polyol Chain Length on Proton Relaxivity of Gadolinium Oxide Nanoparticles for Enhanced Magnetic Resonance Imaging Contrast. *J. Phys. Chem. C* **2019**, *123*, 18061−18070.
(44) Cheah, P.; Zhao, Y. Iron oxide nanoparticles for magnetic resonance imaging with improved sensitivity. In *Nanotechnology: Principles, Applications, and Ethical Considerations*; Ray, P. C., Ed.; Nova Science Publishers, Inc., 2018.

https://dx.doi.org/10.1021/acs.langmuir.0c03314
Langmuir XXXX, XXX, XXX−XXX